Influence of Thermally Aged Underfill on Flip-Chip Packages

Kevin Cox
Tektronix Component Solutions
Beaverton, USA
kevin.cox@tektronix.com

Ghassan Abu-Hamdeh
Tektronix Component Solutions
Beaverton, USA
ghassan.abu-hamdeh@tektronix.com

Matt Borden
Tektronix Component Solutions
Beaverton, USA
matt.borden@tektronix.com

***Abstract*— Underfill material plays a crucial role in flip-chip package reliability, thus it necessary to accurately understand the mechanical properties. The material itself is nonlinear and is dependent on degree of cure, temperature, strain rate and thermal aging, among others. In this work, two underfill materials were characterized for thermal expansion and viscoelastic properties over a wide temperature range. A second set of each material was thermally aged through flip-chip processing steps and 250 thermal cycles and then characterized. Temperature dependent thermal expansion and time-temperature dependent moduli curves were generated to represent each material type. These material models were then implemented into a nonlinear finite element model of a flip-chip package to evaluate package stress interaction through processing steps and thermal cycling. The influence that each underfill material had with and without thermal aging was analyzed with respect to typical package failure mechanisms.**

Keywords—materials characterization, viscoelastic, nonlinear finite element analysis

I. Introduction

Over the last few years, Tektronix Component Solutions (CSO) has been working to advance package reliability through selecting optimal material sets, using best-in-class simulation methods, and refining processing techniques. The reliability of flip-chip packages depends heavily on the underfill (UF) materials used to bond the IC to the substrate. UF plays a crucial role in redistributing mechanical stresses and protecting the chip from environmental factors. Hence, understanding the impact of UF material properties on the reliability of flip-chip packages is paramount. Highly stiff UFs can create excessive stresses on the die and the bonded interface leading to die fracture or UF delamination/fracture, while low stiffness UF don't transfer enough stress and may lead to early C4 fatigue failures or die ULK fractures underneath C4 bumps. In addition to being highly temperature dependent, UF materials are sensitive to the degree of cure, thermal aging, moisture exposure and exhibit creep and viscoelasticity – the modulus is dependent on time (strain rate).

A. Background

The mechanical properties specified on UF technical datasheets can be misleading. For example, the moduli values are often specified for strain rates that are 1-2 orders of magnitude faster than what a typical flip-chip package experiences during thermal cycle qualification testing. This results in poor design and simulation models since the UF modulus and glass transition temperature (T_g) are highly strain rate dependent. In common qualification testing protocols, flip-chip packages are thermally cycled at a rate of 5 C/min (12 sec/C) [1]. A typical UF has a CTE of 30 ppm/C below T_g and 125 ppm/C above T_g. Thus, the thermal strain rate at 5 C/min would be between ~10^{-3} and 10^{-4} % per second. Therefore, it is most relevant to characterize and report UF properties at these strain rates when exploring stresses in flip-chip package processing and thermal cycling conditions. Many studies have been performed previously confirming the significance of UF viscoelasticity as well as thermal aging on package performance [2], [3], [4], [5], [6], [7]. In this work, the focus was on evaluating the UF before and after thermal aging produced from real processing conditions and real thermal cycling qualification loads.

CSO has recently investigated numerous UF material options for optimal performance in advanced-node flip-chip packages. The result of that study identified the two 'best materials" to which further work was required. The follow-on work to identify the best material is described herein. This paper addresses the effects thermal aging on UF coefficient of thermal expansion (CTE) and viscoelasticity and how it influences common flip-chip package failure mechanisms.

The remainder of this section provides an overview of the flip-chip package used for the evaluation. The subsequent sections describe the methods used to characterize the materials and evaluate the impact of thermal aging on key material properties. Thereafter, a nonlinear finite element model and results are discussed which compares how the different UF material properties affected key stress metrics associated with package failure mechanisms CSO has encountered: excessive package warpage, ULK fracture and UF delamination.

B. Description of Package

The device under consideration in this research was an in-house designed advanced node CMOS flip-chip package that goes into a Tektronix product. The package incorporated a 10x8 mm IC with a 180-micron bump pitch and 800-micron BGA pitch on a 25x25 mm substrate. The package geometry is shown in Fig. 1.

II. Methods

This section first describes the materials characterization testing procedure and evaluation techniques. That is followed by a description of the simulation model of the flip-chip package that was created to evaluate key metrics related to critical failure mechanisms.

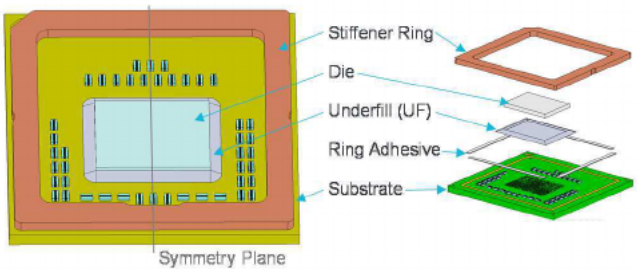

Fig. 1. Description of flip-chip package

TABLE I. MATERIAL GROUP NOMENCLATURE

Material	Thermal treatment	Group
UFA	Cure only	A1
UFA	Cure + thermal aging	A2
UFB	Cure only	B1
UFB	Cure + thermal aging	B2

A. *Materials and preparation*

Material coupons were fabricated for two different UF materials (UFA and UFB). The coupon size was approximately 50x10x4 mm. Each material was divided into two sets: Set 1 (cure only), and Set 2 (cure + thermal aging) to yield 4 unique material sets described in TABLE I.

Curing was performed as described on the UF supplier datasheets. The thermal aging included standard flip-chip processing steps followed by pre-conditioning to MSL 4, and then 250 thermal cycles. Thermal cycling was between 125 C and -40 C with 15-minute dwells at the high/low temperatures and 5 C/min ramp rates. These conditions matched typical processing and qualification test requirements for Tektronix products [1]. Coupon dimensions and masses were recorded before and after thermal cycling to evaluate material shrinkage. Thereafter, the specimens were sent for CTE and rate-dependent modulus (viscoelasticity) testing over a relevant temperature range.

B. *Thermal Expansion Testing*

The CTEs of cured resins have strong dependency on temperature, most notably near their respective glass transition temperatures. To characterize this for UFA and UFB, 10x10 mm square specimens were cut from the prepared coupons and placed in a thermal chamber. The test chamber was purged with nitrogen and was thermally ramped from room temperature to -60 and up to 260 C at a rate of 5 C/min. Specimen displacement was measured with a probe which applied a 50 mN force. Three specimens were tested for each Group. Resulting displacement over temperature curves were generated for each test group.

C. *Viscoelasticity Testing*

To characterize the time-temperature dependency of the material groups, the relaxation moduli were measured at different temperatures across the temperature range. The specimens were loaded in torsion (shear) to 0.01% strain. Force decay was recorded between 0.01 and 600 seconds. Fig. 2 illustrates the force decay method, where the relaxation modulus (a function of time) can be calculated by multiplying the stress (a function of time) and the applied strain (0.01%). The test was run for each specimen at 10 degree C intervals between -60 and 250 C. As previously mentioned, typical strain rates in the UF component (from thermal expansion alone) during thermal cycling are very low. With the 0.01% strain applied in the testing, the UF materials in a package would be best represented by the relaxation moduli values bounded roughly by the 10 to 100-second relaxation times (to yield a strain rate of 0.001% – 0.0001 %/sec). Representative modulus over temperature curves at varying strain rates are shown in Fig. 3 where the influences of relaxation time (strain rate) and temperature are clearly visible.

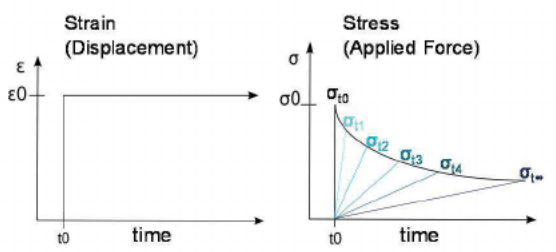

Fig. 2. Stress-relaxation test method

From the test data, time-temperature master curves were generated for each material Group. Each master curve was then fit with a 20-term Prony Series and a Williams-Landel-Ferry shift function. With viscoelasticity and CTE models generated across the full temperature range, each material Group could then be properly represented in the flip-chip simulation model described in the next section.

D. *Simulation Model*

The assembly shown in Fig. 1 was modelled in SolidWorks and imported to ANSYS Mechanical for structural simulations. Due to symmetry, the package was sectioned through the center vertically with respect to Fig. 1 to create a symmetry boundary condition. The structural simulation utilized quadratic elements and large deflections in a multi-step analysis to capture the thermal loading steps involved in flip-chip processing and thermal cycling. The "element birth and death" feature of ANSYS was utilized to "activate" the Stiffener Ring and Ring Adhesive at a specific point during the simulation to match the real-world assembly process. The thermal loading is displayed in Fig. 4. The simulation started with the cure of UF at 165C; the package was at zero stress. The package was cooled to room temperature, relaxed for 15 minutes, then ramped to 165C where the Stiffener Ring and Ring Adhesive became active and bonded to the rest of the package. The package then was cooled room temperature, followed by a thermal cycle from 125 to -40 and back to 125C.

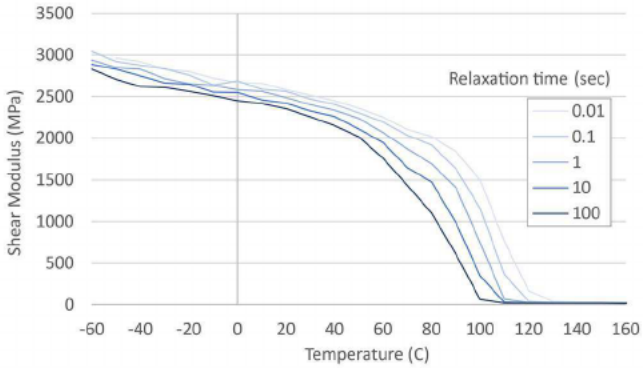

Fig. 3. Shear modulus versus temperature at different relaxation times

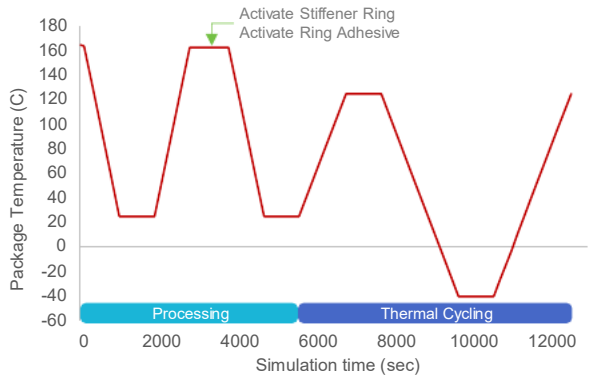

Fig. 4. Thermal Load applied in simulation

A sub-model of a single bump was also designed to provide more accurate results at the corner C4 bump region. Specifically, the sub-model allowed for the extraction of normal stresses in the die back-end-of-line (BEOL) layers and could be used in future studies for C4 bump fatigue predictions. C4 fatigue however was out of scope for this work since that has not been a frequently encountered failure mechanism at CSO. The design of the sub-model is shown beside the global model in Fig. 5 with each component assigned a number that is specified in the materials summary: TABLE II. As is standard for Ansys sub-models, the deformations and stresses came from boundary conditions applied to the circumference of the sub-model which were extracted at every step from the global model displacement results [8]. In addition, the same thermal load from Fig. 4 was applied to the sub-model.

A summary of the material type applied to each component in the global- and sub-model is provided in TABLE II. where temperature-dependent properties are designated with "(T)" and Poisson's ratio is designated with "ν". The die, UF, substrate and ring attach adhesive incorporated temperature dependent CTE values. Material properties for the die BEOL were calculated based on averaging the actual USG, Low-K and ELK stack-up as described in [9]. The UF, ring attach adhesive and substrate moduli values were derived from the respective material's time-temperature master curves and were each represented in ANSYS by a multi-term Prony Series and a Williams-Landel-Ferry shift function.

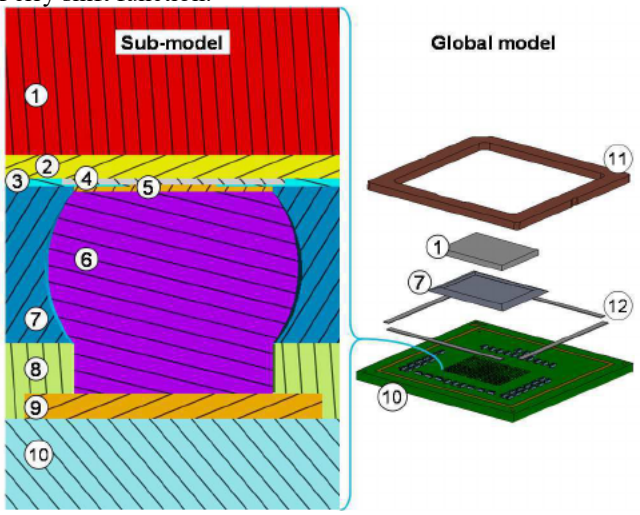

Fig. 5. Simulation sub-model and component identification #

TABLE II. SUMMARY OF MATERIALS IN SIMULATION MODEL

#	Component	Material	Key Properties
1	Die (bulk)	Silicon	Orthotropic Modulus, CTE(T), ν
2	Die BEOL	Composite	Orthotropic Modulus Orthotropic CTE, ν
3	Die Passivation	Polyimide	Modulus, CTE, ν
4	Die C4 Pad	Aluminum	Modulus, CTE, ν
5	Die UBM	Copper	Bilinear Modulus, CTE, ν
6	Solder Bumps	SnAg	Viscoplasticity(T), CTE, ν
7	Underfill	Thermoset Resin	Viscoelasticity(T), CTE(T), ν
8	Substrate Solder Mask	Thermoset	Modulus(T), CTE(T), ν
9	Substrate C4 Pad	Copper	Bilinear Modulus, CTE, ν
10	Substrate	Composite	Viscoelasticity(T), CTE, ν
11	Stiffener Ring	Copper	Modulus, CTE, ν
12	Ring Adhesive	Thermoset	Viscoelasticity(T), CTE(T), ν

Like the UF materials, the substrate and ring attach adhesive master curves were developed by performing stress-relaxation testing over the relevant temperature range; however, the influence of aging on these materials was out of scope in this work. The substrate, due to its orthotropic nature, required performing testing in both in-plane directions. Finally, the solder bumps incorporated Anand viscoplastic properties [10]. Additional details about the simulation model are provided in [11].

III. RESULTS AND DISCUSSION

In this section, results from the material characterization tests are discussed first followed by the simulation results.

A. Material Characterization Tests

1) Physical Properties

The length, width, thickness, and mass of each test specimen was recorded before and after thermal aging. With the length of the coupon being the largest dimension, it represented the best metric for comparison since it minimized influence of measurement tool uncertainty. Four specimens were measured for each group. As shown in TABLE III. , thermal aging imparted no significant shrinkage or change in mass after the initial cure. The values in the table show percent change with respect to A1 (row 2) and B1 (row 3).

TABLE III. CHANGES TO SPECIMEN DIMENSIONS AND MASS AFTER THERMAL AGING

Group	Delta Length	Delta Mass
A2	+0.08%	+0.05%
B2	-0.05%	-0.17%

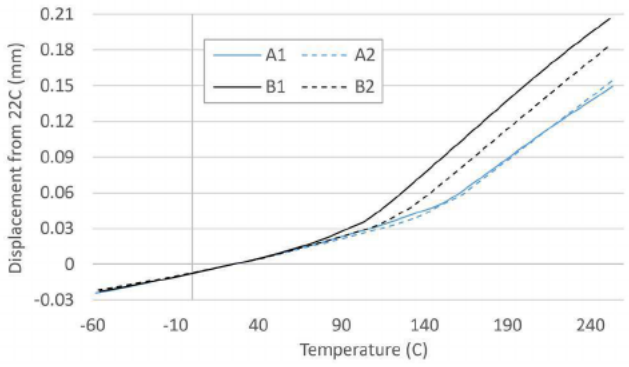

Fig. 6. Thermal expansion versus temperature for all groups

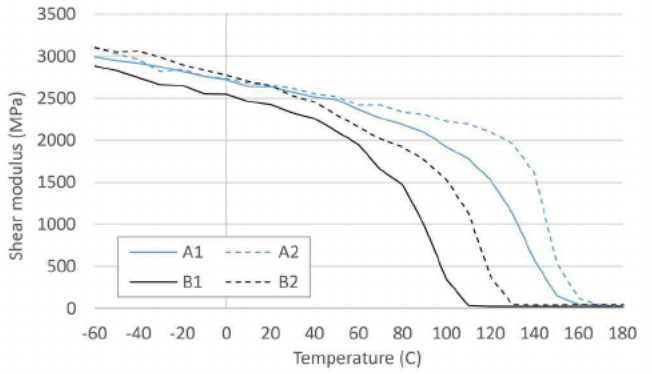

Fig. 7. Shear modulus over temperature for all groups at 10 seconds relaxtion time

2) Thermal Expansion

Specimen displacement for each material group is plotted in Fig. 6 across the relevant temperature range with displacements taken relative to Room Temperature. Each curve represents the average response of the 3 coupons tested in each group. The slope of the curve at any specific temperature is equal to the material's CTE. All curves exhibited typical responses for cured resins: bilinear behavior with a lower CTE (flatter slope) below T_g and a higher CTE (steeper slope) above T_g. TABLE IV. summarizes the changes to the average CTE between -40 and 125C after thermal aging. In the table 4th column, B1 is calculated with respect to A1 and B2 is with respect to A2.

Material A exhibited a stable response with respect to thermal aging; both CTE and T_g remained within close proximity of the initial, as-cured properties. Material B exhibited a strong dependency on thermal aging; the T_g increased by 16% and because of this, the average CTE between -40 and 125 C decreased by 19%. This is a rather common occurrence for thermosetting resins: additional heat and time may further increase a resin's cross-linking which yields a stiffer, more brittle material with a higher T_g and a lower CTE.

From a package reliability perspective, low CTE and high T_g are typically good traits for UF materials. In this regard, the results showed that while UFB improved after thermal aging, it never became as good as UFA. UFA was therefore preferrable for this aspect, and the fact that it was more stable makes it easier and more predictable to work with.

3) Viscoelasticity

To provide a simple visual comparison, Fig. 7 shows the relaxation moduli versus temperature plotted for the different material groups at a single relaxation time (10 seconds). TABLE V. shows the average shear modulus of the materials between -40 and +125 C.

TABLE IV. CHANGE TO AVERAGE CTE AFTER THERMAL AGING

Group	Avg CTE (ppm/C)	Change from cure only	Change from UFA
A1	34.9	---	---
A2	33.1	-5.2% -1.8 ppm/C	---
B1	46.6	---	+33.6%
B2	37.4	-19.6% -9.1 ppm/C	+13.3%

Thermal aging increased T_g for UFA by ~15 C and decreased the span of the T_g transition region, while the modulus stayed rather constant outside of the transition region. For UFB, thermal aging increased the modulus consistently across all temperatures as well as shifted the Tg higher by ~20 C. When comparing UFA and UFB, again it was clear that UFA was less influenced by thermal aging. Before aging, UFB had lower T_g and moduli at all temperatures especially in the transition region. After thermal aging, the moduli were similar below 40C. Above 40C, UFA was stiffer, exhibited a higher T_g and a narrower transition zone.

B. Simulation

Results from both the global model and sub-model are described in this section. The global model provided die (and package) deflections and peak stresses on the BEOL layer near the die corners. Stress on the BEOL was taken on the surface in contact with the UF as a metric for delamination at this interface. The sub-model provided results at the corner C4 bump region for BEOL fracture (ULK fracture or delamination). The most significant stress in BEOL layers is in the normal (through-thickness) direction as described in [9], [12]. The results are summarized in the following sub-sections.

1) Package deflection

Characteristic package warpage (displacement in the through-thickness direction) is shown at -40 C (maximum deflection) in Fig. 8. Values of the die warpage (maximum – minimum) were recorded for each material group at -40 C and are presented in TABLE VI. The change in die deflection due to thermally aged UF properties was rather minor with UFA and UFB deflections both changing by less than 5%. A clearer result was that UFB produced less warpage, possibly because it was softer and thereby allowed for more shear strain between the die and substrate which reduced bending magnitude.

TABLE V. CHANGE TO SHEAR MODULUS AFTER THERMAL AGING

Group	Avg Shear Modulus (MPa)	Change from cure only	Change from UFA
A1	2407	---	---
A2	2523	+4.8%	---
B1	1795	---	-25.4%
B2	2196	+22.3%	-13.0%

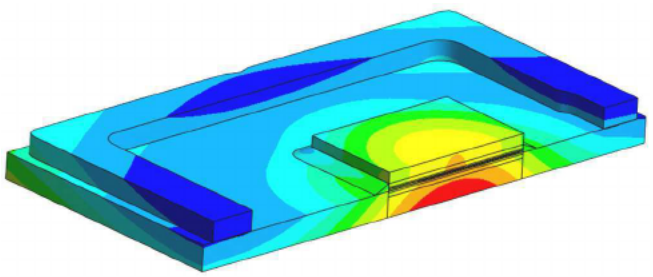

Fig. 8. Package warpage (deflection in thickness direction)

TABLE VI. CHANGES TO DIE WARPAGE AFTER THERMAL AGING

Group	Die Warpage (mm)	Change from cure only	Change from UFA
A1	29.6	---	---
A2	28.8	-2.9%	---
B1	25.2	---	-14.8%
B2	26.3	+4.1%	-8.7%

2) Delamination Stress

Stress on the BEOL component was recorded near the corner of the die: the specific location is represented by the orange triangle region shown in Fig. 9. As shown in the figure, the region did not extend all the way to the die edges/corner to avoid influence from stress singularities at the (component's) corner nodes. The stress results are presented in TABLE VII. The maximum principal stress was selected as the stress metric since delamination at this surface would likely be due to (in-plane or through-thickness) tensile loads.

UFA was found to produce lower delamination stresses than UFB both before and after thermal aging. Thermal aging increased the UFA BEOL stress by ~6%. Considering UFB, the delamination stress remained nearly constant after thermal aging. This was a surprising result since major changes were found from material testing before and after thermal aging, with average CTE decreasing ~20% and average modulus increasing ~22%. It appeared that these changes may have offset each other. However it isn't as simple as comparing average values since T_g and ramp rates also played important roles. Furthermore, the substrate and C4 bump materials also had their own complex behaviors which, together with all the other components, contributed to highly complex package stress interactions.

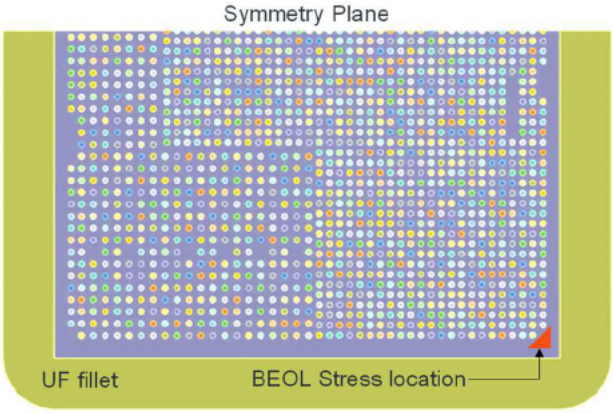

Fig. 9. Location of delamination stress metric on BEOL surface

TABLE VII. CHANGES TO DELAMINATION MAX PRINCIPAL STRESS AFTER THERMAL AGING

Material	Delamination Max Principal Stress (MPa)	Change from cure only	Change from UFA
A1	71.1	---	---
A2	75.3	+5.9%	---
B1	80.3	---	+12.9%
B2	79.5	-1.0%	+5.6%

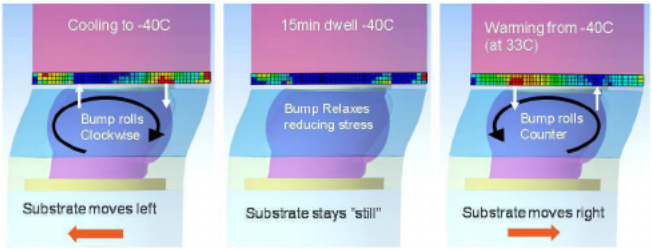

Fig. 10. Cross-section of normal stress in BEOL layers at corner C4 bump

3) BEOL fracture

A summary of the maximum through-thickness stress in the BEOL layers is presented in TABLE VIII. Through the simulation load steps, the location of maximum normal stress depended on whether the package was heating up or cooling down as depicted in Fig. 10. The normal stress was created from the moment applied by the C4 bump to the BEOL. The influence of dwell time can clearly be seen between the left and center images where the solder relaxed (creeped) under the high load, and thereby reduced the BEOL stress. Upon heating from -40C, the maximum normal stress moved to the opposite side of the bump and approached a similar but smaller magnitude as that found at -40 C.

Thermal aging increased BEOL stress for both UFA and UFB. Reductions in UF CTE after aging meant less vertical compression to the solder bumps when cooling the package and also less compression to the C4 pad and BEOL layer. This could be one reason why BEOL normal stresses increased. As was found for delamination stress, UFA with its lower average CTE and higher average modulus than UFB yielded lower BEOL normal stresses both before and after thermal aging.

IV. SUMMARY AND CONCLUSIONS

Two materials were considered for a flip-chip package UF. This work characterized the CTE and viscoelasticity of each UF before and after thermal aging to understand how the mechanical properties of the materials changed over time. Temperature-dependent CTE curves and Time-Temperature dependent moduli curves were created to represent the materials in nonlinear finite element simulations.

TABLE VIII. CHANGES TO BEOL NORMAL STRESS AFTER AGING

Material	BEOL Normal Stress (MPa)	Change from cure only	change from UFA
A1	38.0	---	---
A2	40.8	+7.2%	---
B1	42.1	---	+10.7%
B2	44.4	+5.4%	+8.9%

The simulations incorporated the materials into the Underfill component of an advanced node CMOS flip-chip package. The model included relevant processing loads followed by a thermal cycle that the device would experience in qualification testing. The simulation output metrics associated with common critical failure mechanisms in flip-chip packages and provided an understanding of the influence thermal aging had on each material and the determination of which material was best. Thermally aging the UF materials influenced key mechanical properties by up to ~20%, while critical package stress results were influenced by ~5 – 10%. The following conclusions were made:

- Thermal aging did not impart a significant shrinkage or change in mass to either UF material.
- The CTE of UFA was lower and remained lower than UFB after thermal aging. The CTE and of UFB was significantly influenced by thermal aging, reducing almost 20% from its initial value.
- It was found from viscoelasticity characterizations that thermal aging increased T_g for UFA by ~15C. For UFB, aging increased the modulus consistently across all temperatures as well as shifted the $T_g$higher by ~20 C. UFA was the stiffer material.
- UFA was less influenced by thermal aging than UFB.
- Thermal aging did not have a major influence on die warpage.
- UFA performed better in both simulation stress metrics for both the pristine and thermally aged material states. However, UFB yielded a package with less warpage.
- Package performance with UFB generally improved after thermal aging with respect to simulated failure metrics, but never matched the performance provided by UFA.

REFERENCES

[1] JEDEC JESD22-A104F.01, "Temperature Cycling," 2023.

[2] Z. Qian, J. Wang, J. Yang and S. Liu, "Visco-elastic-Plastic Properties and Constitutive Modeling of Underfills," *IEEE Transactions on Components and Packaging Technologies,* vol. 22, no. 2, pp. 152-157, 1999.

[3] F. Feutsel, S. Wiese and E. Meusel, "Time-dependent material modeling for finite-element analyses of flip chips," *Proc. of 52nd Electrical Components Technologies Conference,* pp. 1548-1553, 2000.

[4] C. Lin, J. C. Suhling and P. Lall, "Evolution of the stress-strain and creep behavior of underfill encapsulants with aging," *Proceedings ASME 2009 InterPACK Conference,* 2009.

[5] F. X. Che, X. R. Zhang and L. Ji, "Thermal Aging Induced Underfill Degradation and Its Effect on Reliability of Advanced Packaging," *IEEE 70th Electronic Components and Technology Conference,* pp. 1525-1532, 2020.

[6] X. Q. Shi, Y. L. Zhang, W. Zhou and X. J. Fan, "Effect of Hygrothermal Aging on Interfactial Reliability of Silicon/Underfill/FR-4 Assembly," *IEEE Transactions on components and packaging technologies,* vol. 31, no. 00, pp. 94-103, 2008.

[7] P. Lall, M. Kasturi, Y. Zhang, H. Wu, J. Suhling and E. David, "Effect of Underfill Property Evolution on Solder Joint Reliability in Automotice Applications," *Proceedings of the IEEE Electronic Components and Technology Conference,* pp. 456-466, 2022.

[8] T. Zhang, S. Rahman, K. K. Choi, K. Cho, P. Baker, M. Shakil and D. Heitkamp, "A Global-Local Approach for Mechanical Deformation and Fatigue Durability of Microelectronic Packaging Systems," *Journal of Electronic Packaging,* vol. 127, pp. 179-189, 2007.

[9] M. Gonzales, B. Vandevelde, A. Ivankovic, V. Cherman, B. Debecker, M. Lofrano, I. De Wolf, G. Beyer, B. Swinnen, Z. Tokei and E. Beyne, "Chip Package Interaction (CPI): Thermo Mechanical challenges in 3D Technologies," *IEEE 14th Electronics Packaging Technology Conference,* pp. 547-551, 2012.

[10] Z. Cheng, L. Wang, J. Wilde and K. Becker, "Viscoplastic Anand Model for Solder alloys and its application," *Soldering & Surface Mount Technology,* vol. 12, pp. 31-36, 2000.

[11] K. Cox, J. Krantz, M. Borden and S. Tonthat, "Validating Flip Chip package models through experimental deflection measurements," in *IMAPS Device Packaging Conference*, Fountain Hills, 2023.

[12] M. Lane, "Interface Fracture," *Annual Review of Materials Research,* vol. 33, pp. 29-54, 2003.